#### Research Article

Lushuai Cao, Tuanhui Jiang, Bujin Liu, Ming Li, Di Zhang, Wei Gong\*, and Li He\*

# Effects of grafting and long-chain branching structures on rheological behavior, crystallization properties, foaming performance, and mechanical properties of polyamide 6

https://doi.org/10.1515/epoly-2022-0030 received December 07, 2021; accepted January 22, 2022

**Abstract:** Polyamide 6 (PA6) was modified with ethylene maleic anhydride syndiotactic copolymer resin (ZeMac), and triglycidyl isocyanurate (TGIC) as modifiers to prepare a grafting structure and a long-chain branching structure, respectively. The effects of two modifiers on the rheological behavior, crystallization properties, foaming performance, and mechanical properties of PA6 were systematically studied by rotating rheometry, differential scanning calorimetry and scanning electron microscopy. The results showed that there were differences in crystallization properties between the two modification methods, but they significantly improved the rheological, foaming performance, and mechanical properties of PA6. In particular, PA6 with long-chain branching structure through TGIC modification showed better performance in various physicochemical characterizations. The introduction of ZeMac reduced the average diameter of bubbles in pure PA6 from 146.32 to 88.12 µm, and the density of bubbles increased from  $1.69 \times 10^5$  to  $5.35 \times 10^5$  cells·cm<sup>-3</sup>. The introduction of TGIC reduced the average diameter of bubbles in pure PA6 from 146.32 to 64.36 µm, and the density of bubbles

**Keywords:** polyamide 6, grafting structure, long-chain branching structure, rheological behavior, foaming performance

# 1 Introduction

Polymer foam as an excellent lightweight material is widely used in the fields of household appliances, automobiles, building materials, and so on due to its characteristics of low energy consumption, low cost, high energy absorption, sound insulation, and heat insulation (1-5). In general, the properties of polymer foams mainly depend on the cell structure, such as cell size, cell size distribution, and cell density, which is mainly determined by molecular structure of the polymer and rheological behavior of the melt (6,7). Polyamide 6 (PA6), as an important semicrystalline thermoplastic engineering plastic, has many excellent properties, such as high stiffness, wear resistance, self-lubricating, and chemical resistance. It has attracted extensive attention in industrial application and academic research (8,9). However, the linear molecular chain structure and low melt strength of PA6 seriously restricts its application in thermoforming, blowing, and foaming where elongational deformation is dominant. Therefore, the modification of PA6 becomes particularly important to expand its application. In addition, PA6 is highly sensitive to crack propagation and shows brittle fracture behavior in the process of tension and impact, which limits its application in many load-bearing fields.

Researchers have developed various methods to overcome the problem of low foaming quality caused by low melt strength, such as adding fiber (10), rubber (11), and inorganic particles (12). However, the dispersed phase of the above method has the characteristics of difficult uniform

**Di Zhang:** School of Chemistry and Chemical Engineering of Guizhou University, Guiyang, China; National Engineering Research Center for Compounding and Modification of Polymer Materials, Guiyang, China

increased to  $1.31 \times 10^6$  cells·cm<sup>-3</sup>. Moreover, the mechanical properties of both nonfoamed and foamed samples were improved after modification.

<sup>\*</sup> Corresponding author: Wei Gong, The Institute of Materials and Construction of Guizhou Normal University, Guiyang, China, e-mail: gw20030501@163.com

<sup>\*</sup> Corresponding author: Li He, College of Materials and Metallurgy of Guizhou University, Guiyang, China; National Engineering Research Center for Compounding and Modification of Polymer Materials, Guiyang, China, e-mail: lihe@gzu.edu.cn

Lushuai Cao, Tuanhui Jiang, Bujin Liu, Ming Li: College of Materials and Metallurgy of Guizhou University, Guiyang, China; National Engineering Research Center for Compounding and Modification of Polymer Materials, Guiyang, China

dispersion and easy agglomeration, which will cause stress concentration and inevitably reduce the strength of the material (13,14). Chemical modification is a promising method because it can improve the melt strength of materials without introducing phase separation. In recent years, researchers have improved the rheological behavior and foaming performance of polymer materials through different chemical modification methods, such as crosslinking (15,16), grafting (17–19), and long-chain branching (20–22). Li et al. (23) prepared the modified polylactic acid with longchain branched (LCB) structure by introducing epoxy organic peroxide, which significantly improved the melt strength and crystallization properties of polylactic acid. Jiang et al. (21) controllably prepared LCB polylactic acid by reacting a linear thermoplastic polyester elastomer (TPEE) with triglycidyl isocyanurate (TGIC) and 2,2'-bis(2-oxazoline) (2,2'-boz) in different order thermoplastic polyester elastomer (TPEE) to improve its rheological behavior and foaming ability. Leng et al. (18) synthesized three series of vulcanized branched polylactic acid. In addition, they pointed out that the increase of grafting length and grafting density will improve zero viscosity  $(\eta_0)$  and enhance complex module  $(g^*)$ , in which the enhancement effect of grafting density on rheological behavior is greater than that of grafting length. Xu et al. (24) studied the effects of star and tree structure on the rheological behavior and foaming window of PA6 with adr-4368 and maleic anhydride-grafted polypropylene as modifiers. Compared with chain extended PA6, the LCB-PA6 showed much higher shear viscosity and longer characteristic relaxation times. As noted, the chain length and branching degree strongly affect the chain motion in the polymer melt and determine the rheological behavior of the polymer. Many researchers have adopted the method of adding reactive chain extenders to form grafting structure or long-chain branching structure to improve the material properties. However, this is something that needs to be further explored for the differences in material properties and foaming performance between the two structures, which are extremely important for selecting appropriate modification methods in practical application. The longchain branching has a more complex structure compared with grafting because long-chain branching structure not only increases the degree of molecular chain branching but also increases the length of main chain and branch chain. The difference of molecular chain structure mentioned above will have different effects in various physicochemical characterizations of the polymer. In this study, PA6 was modified with ZeMac and TGIC as modifiers to prepare a grafting structure and a long-chain branching structure respectively. The effects and differences of grafting and

long-chain branching structures were investigated on rheological behavior, crystallization properties, foaming performance, and mechanical properties.

# 2 Experiment

#### 2.1 Materials

Polyamide 6 (PA6: m 2400, melt index of 26 g·10 min<sup>-1</sup> (235°C, 2.16 kg), density of 1.54 g·cm<sup>-3</sup>) was obtained from Guangdong Xinhui Meida Co., Ltd. Chemical foaming agent F-70 (gas production volume: 35 mL·g<sup>-1</sup>; the main components were polyethylene and sodium bicarbonate) was obtained from Eiwa Chemical Ind. Co., Ltd, Japan. TGIC was provided by Huangshan Taida Chemical Company, P. R. China. Ethylene maleic anhydride syndiotactic copolymer resin (ZeMac) was provided by Shanghai Nasu Alloy Technology Co., Ltd. Table 1 shows the chemical structures of the two modifiers. All were used as received without any further treatments.

# 2.2 Sample preparation

PA6 particles were dried in an oven at 105°C for 4 h, and then PA6 was mixed with ZeMac and TGIC at a certain mass fraction (Table 2) and extruded at a screw speed of 250 rpm using a twin-screw extruder to prepare modified PA6 samples (CTE20, Kebeilong Keya (Nanjing) Machinery Co., Ltd). The obtained modified PA6 granules were dried in the oven at 105°C for 4 h. Then the mixture of modified PA6 samples and foaming masterbatch in a mass ratio of 98:2 was added to the injection hopper to prepare foam samples in an injection molding machine (EM120-V, Zhende Plastic Machinery Co., Ltd). The temperature of each section

Table 1: Chemical structures of modifiers used in this work

Agents	Chemical structures	Characteristics
ZeMac-L68	0 0 0	Content of MAH: >78% Molecular weight: 40,000 g·mol <sup>-1</sup>
TGIC		Purity: 98% Molecular weight: 297.26 g·mol <sup>-1</sup>

Table 2: Weight percentages of materials

Samples	PA6 (wt%)	ZeMac (wt%)	TGIC (wt%)
Pure PA6	100	0	0
PA6-ZeMac 0.3	99.7	0.3	0
PA6-ZeMac 0.5	99.5	0.5	0
PA6-ZeMac 0.7	99.3	0.7	0
PA6-TGIC 0.3	99.7	0	0.3
PA6-TGIC 0.5	99.5	0	0.5
PA6-TGIC 0.7	99.3	0	0.7

of the injection molding machine from hopper to the die was set from 220°C to 240°C. The initial cavity thickness of the nonfoamed sample was 4 mm, and the mold was not opened. The initial cavity thickness of the foamed sample was 3.2 mm, and core-back distance was 0.8 mm.

# 2.3 Testing and characterization

# 2.3.1 Attenuated total reflection-Fourier transform infrared (ATR-FTIR) spectroscopy

FTIR spectroscopy (Nicolet-6700, Nicolet, USA) was used to characterize the reaction between pure PA6 terminal group and ZeMac-L68 and TGIC functional groups. A few samples were directly taken and put in the ATR detection window, the probe was aligned with the detection window, and then pressed for detection.

#### 2.3.2 Gel permeation chromatography (GPC)

GPC was tested with Agilent PL-GPC 50. First, hexafluor-oisopropanol (HFIP) was used to prepare a sample with a concentration of 1.0  $mg\cdot mL^{-1}$ , heated to 40°C for dissolution, and then tested at 40°C with a flow rate of 1  $mL\cdot min^{-1}$ . The chromatographic column was PL 1114-6900 HFIP. The solution was filtered with 0.1  $\mu$ m filter paper, and then the filter paper was dried and weighed to determine whether cross-linking occurred before the experiment. It was found that there was no change in the mass before and after, so it was determined that there was no crosslinking.

#### 2.3.3 Rheological behavior

A rotational rheometer (HAAKE MARS 60) with parallel plate geometry was used to measure the dynamic shear rheological behavior and uniaxial tensile rheological behavior of the virgin and modified PA6. The mold cavity volume

was adjusted by core-back to prepare the samples with a thickness of 1.0 mm, and then a small circle with a diameter of 20 mm and a thickness of 1.0 mm was taken. Dynamic strain sweep tests were conducted to identify the strain limits of the linear viscoelastic region. The oscillation frequency sweep tests were performed in a nitrogen atmosphere at 225°C and with a pre-set strain of 1% in the linear viscoelastic to determine the viscoelastic properties. Characterizing the storage modulus G', the loss modulus G'', and the complex viscosity  $\eta^*$  as a function of angular frequency  $\omega$ (0.3–100 rad·s<sup>-1</sup>). The mold cavity volume was adjusted by core-back to prepare a 1.0 mm thick spline, and then a small cuboid with a length of 25 mm, a width of 10 mm, and a thickness of 1.0 mm was taken for the uniaxial elongational viscosity tests. The rheological behavior of uniaxial elongation was tested using the SER tool in a nitrogen atmosphere at 225°C. The strain rate in this experiment is  $0.05 \,\mathrm{s}^{-1}$ .

#### 2.3.4 Crystallization properties

Differential scanning calorimeter (DSC, TA Q25, New Castle, DE, USA) was used to test the melting and crystallization parameters of samples under nitrogen atmosphere. The sample was first heated rapidly from 30°C to 240°C in a nitrogen atmosphere for 3 min to eliminate the thermal history, then cooled at 20°C·min<sup>-1</sup> to 30°C, and finally heated at 20°C·min<sup>-1</sup> to 240°C. The crystallization and melting curves were obtained by the above process.

The calculation formula of crystallinity is shown in Eq. 1:

$$X_{\rm C} = \frac{\Delta H_{\rm f}}{\Delta H_{\rm f}^0 \times w} \times 100\% \tag{1}$$

where  $X_C$  is the degree of crystallinity, %;  $\Delta H_f$  is the enthalpy of fusion of the sample,  $g \cdot J^{-1}$ ;  $\Delta H_f^0$  is the standard enthalpy of PA6 100% crystallization, 190  $g \cdot J^{-1}$ ; and w is the PA6 matrix's weight fraction.

The crystal morphology was observed by a polarizing microscope (POM, Olympus BX51) equipped with a hot stage. The pure PA6 and modified samples were first melted at 240°C for 5 min, then cooled to 195°C at a rate of 50°C·min<sup>-1</sup>, and maintained at this temperature for isothermal crystallization, and photographs were taken at different times.

#### 2.3.5 Characterization of foaming performance

The sample was notched and put into liquid nitrogen soaked for 3 h. It was immediately punched after taking

out and the surface was sprayed with gold. The cell morphology of the microcellular foamed PA6 composites was observed by a scanning electron microscope (SEM; EM 6200, Beijing China Science and Technology Instrument Co., Ltd). Pictures of cell structure were taken at different multiples. The diameter of the cells and the number of cells were calculated by the Image Plus software. The bubble density was calculated by Eqs. 2 and 3 as shown below:

$$N_0 = \left[\frac{n}{A}\right]^{\frac{3}{2}} \left[\frac{1}{1 - V_f}\right] \tag{2}$$

$$V_{\rm f} = 1 - \frac{\rho_{\rm f}}{\rho_{\rm o}} \tag{3}$$

where  $N_0$  is the cell density, cell·cm<sup>-3</sup>;  $V_f$  is the porosity;  $\rho_0$  and  $\rho_f$  are the apparent densities of samples before and after foaming process, respectively; n is the number of cells in the SEM image; and A is the micrograph area, cm<sup>2</sup>.

#### 2.3.6 Mechanical property

The tensile properties were measured according to GB/T 1040.2-2006 by an electronic universal testing machine (CMT 6104, Meister industrial systems (China) Co., Ltd), with the tensile speed of 50 mm·min<sup>-1</sup>. The impact

performance was tested according to GB/T 1843 by a pendulum impact testing machine (ZBC-4B, Shenzhen Xinsansi Measurement Technology Co., Ltd). The notch depth of the sample was 2 mm, and the impact energy of the pendulum was 2.75 J. The values were averaged out over five measurements.

# 3 Results and discussion

#### 3.1 Reaction evolution

Scheme 1 shows the chain extension mechanism of ZeMac and TGIC as modifiers to PA6. Two branched extenders of different lengths (comb-like shape and tree-like shape) are formed. For the reaction between ZeMac and PA6, PA6 has only amino groups involved in the reaction. The active hydrogen on the amino group at the end of PA6 attacks the carbon oxygen bond on ZeMac maleic anhydride to generate ring opening reaction, which make PA6 grafting on the ZeMac molecular chain to from the grafting product of ZeMac-PA6. The comb ZeMac-PA6 chain extension structure is obtained when more PA6 is grafted on ZeMac by chain extension. For the reaction between TGIC and PA6, both amino and carboxyl groups of PA6 will participate in

Scheme 1: The reaction diagrams of the two modification methods and the possible product chain structure.

the reaction. The active hydrogen on the amino or carboxyl group at the end of PA6 attacks the carbon oxygen bond on the epoxy group of TGIC to open the epoxy group, which generates the chain extension product of TGIC-PA6 with three arm comb shape. Then, the end group of the product can continue to react with TGIC, and finally form a dendritic TGIC-PA6 LCB structure.

In order to verify the rationality of the mechanism, Figure 1 shows the FTIR of the following substances: ZeMac, TGIC, pure PA6, PA6-ZeMac 0.5, and PA6-TGIC 0.5. Among, the peaks of 1,702 and 1,248 cm<sup>-1</sup> on the ZeMac are the characteristic stretching vibration peak of conjugated carbonyl of maleic anhydride group and the stretching vibration peak of ether bond respectively. However, it is worth noting that the peaks for PA6-ZeMac 0.5 at 1,702 and 1,248 cm<sup>-1</sup> disappear, which proves that maleic anhydride on ZeMac has been opened and reacted with the amino group on PA6. The peaks of 1,637 and 1,535 cm<sup>-1</sup> on pure PA6 correspond to the amide group, and 928 cm<sup>-1</sup> corresponds to the bending vibration of hydroxyl. It is reported that the epoxy group region of TGIC is  $910-950 \,\mathrm{cm}^{-1}$  (24). Therefore, the peak at  $926 \,\mathrm{cm}^{-1}$ is the carbon-oxygen tensile vibration peak in the epoxy group, but this peak is not observed in PA6-TGIC 0.5, reflecting that the epoxy group of TGIC has been consumed. The hydroxyl group peak of pure PA6 disappeared at 928 cm<sup>-1</sup>, which reflected that the carboxyl terminal group of pure PA6 participated in the reaction. Figure 2 shows the molecular weight distribution of pure PA6, PA6-ZeMac 0.5, and PA6-TGIC 0.5. Table 3 shows the detailed data of molecular weight and dispersion index  $M_W/M_p$ . As shown in Figure 2, the addition of ZeMac or TGIC modifier moves the curve to the high molecular weight region, which means

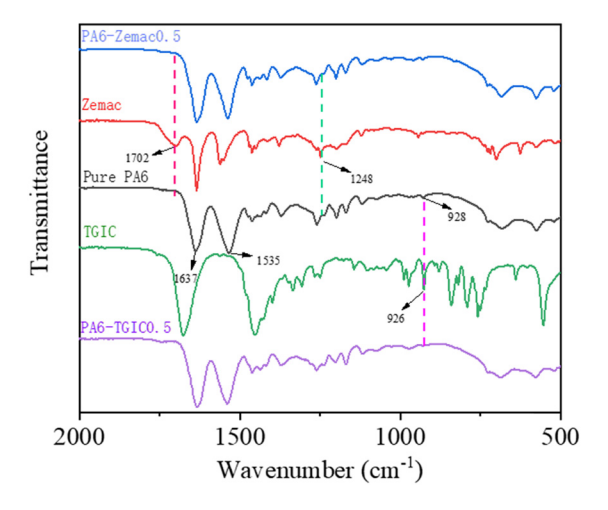


**Figure 1:** FTIR spectra of ZeMac, TGIC, pure PA6, PA6-ZeMac 0.5, and PA6-TGIC 0.5.

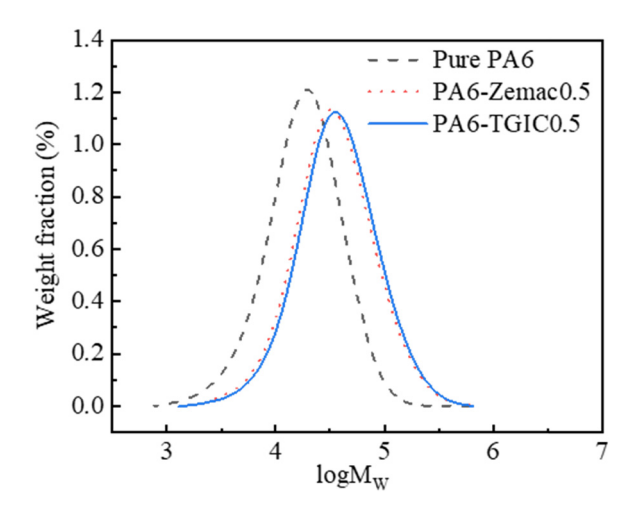


Figure 2: Molecular weight distributions of the pure PA6, PA6-ZeMac, and PA6-TGIC 0.5.

that both modifiers react with PA6 and improve the molecular weight of the material. In general,  $M_{\rm W}$  is greatly affected by the high molecular weight in the polymer. As shown in Table 3, PA6-TGIC 0.5 with LCB structure has higher  $M_{\rm W}$  compared with PA6-ZeMac 0.5 with a grafting structure, indicating that the LCB structure is conducive to the formation of entangled macromolecules and higher molecular weight.  $M_{\rm n}$  is related to the end cardinality and the number of entanglements on each chain, indicating that the tree structure consumes more end groups than the comb structure, and there are more entanglements in the chain. The more entangled molecular chains, the greater the intermolecular force, making the higher the melt viscosity and melt strength (24).

# 3.2 Rheological behavior

Some studies have shown that increasing the viscoelasticity and melt strength of polymer is helpful to promote cell nucleation and stabilize cell structure (25–28). Figure 3a–c shows the storage modulus (G'), loss modulus (G''), and loss tangent angle ( $\tan \delta$ ) of PA6-ZeMac and PA6-TGIC, respectively. The G' and G'' of PA6 ZeMac and PA6-TGIC gradually increase with the increase of modifier content in the whole frequency scanning range as shown in Figure 3. The G' reflects the elasticity of the material, and the G'' reflects the viscosity of the material. Therefore, the melt viscoelasticity of PA6 is improved with the addition of two modifiers. Some molecular chain information can be reflected through G' curve. PA6-TGIC0.5 and PA6-TGIC0.7 have a relaxation process in the low-frequency region,

Table 3: Molecular properties of the pure PA6, PA6-ZeMac, and PA6-TGIC 0.5

Samples $M_{\rm w} ({\rm kg \cdot mol}^{-1})$		M <sub>n</sub> (kg·mol <sup>-1</sup> )	Mz (kg·mol <sup>-1</sup> )	$M_{\rm w}/M_{\rm n}$
Pure PA6	23.8	13.4	39.2	1.78
PA6-ZeMac 0.5	44.4	22.5	86.5	1.97
PA6-TGIC 0.5	48.9	23.2	92.9	2.11

which is related to the formation of more LCB structures in the reaction process. In addition, compared with pure PA6, the modified sample has a slower relaxation rate in the terminal region, which indicates that it has more branched structure and longer molecular chain (29). The  $\tan \delta$  reflects the relative size of the viscosity and elasticity of the material. The larger the  $\tan \delta$ , the greater the viscosity of the material is, and the smaller the  $\tan \delta$ , the greater the elasticity of the material is (30). It can be seen from Figure 3c that the  $\tan \delta$  of PA6 gradually decreases with the increase of modifier content, especially when the TGIC content is high, indicating that the introduction of the

modifier improves the viscoelasticity of PA6. In addition, it is found that TGIC has a more significant effect on the viscoelasticity of PA6 by comparing the effects of the two modifiers. The above difference is due to the different modification mechanisms of ZeMac and TGIC on PA6 (Scheme 1). The modification method of ZeMac is grafting. The molecular chain of PA6 is grafted on the molecular chain of ZeMac to increase the degree of molecular chain branching, and finally form a comb structure. The modifier TGIC further improved the length and topological structure of the branched chain while improving the degree of branched chain, forming a tree structure, increasing the entanglement

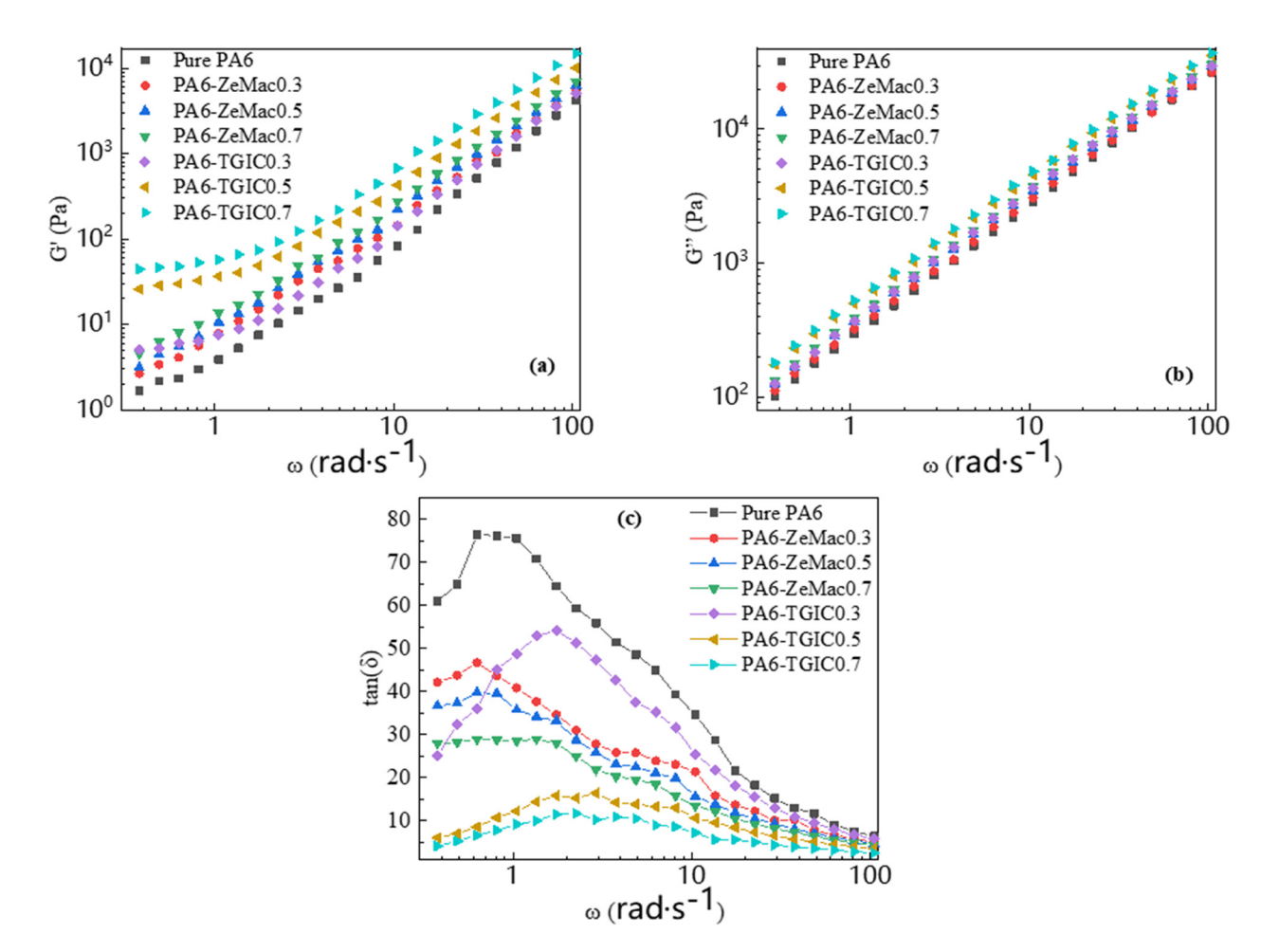
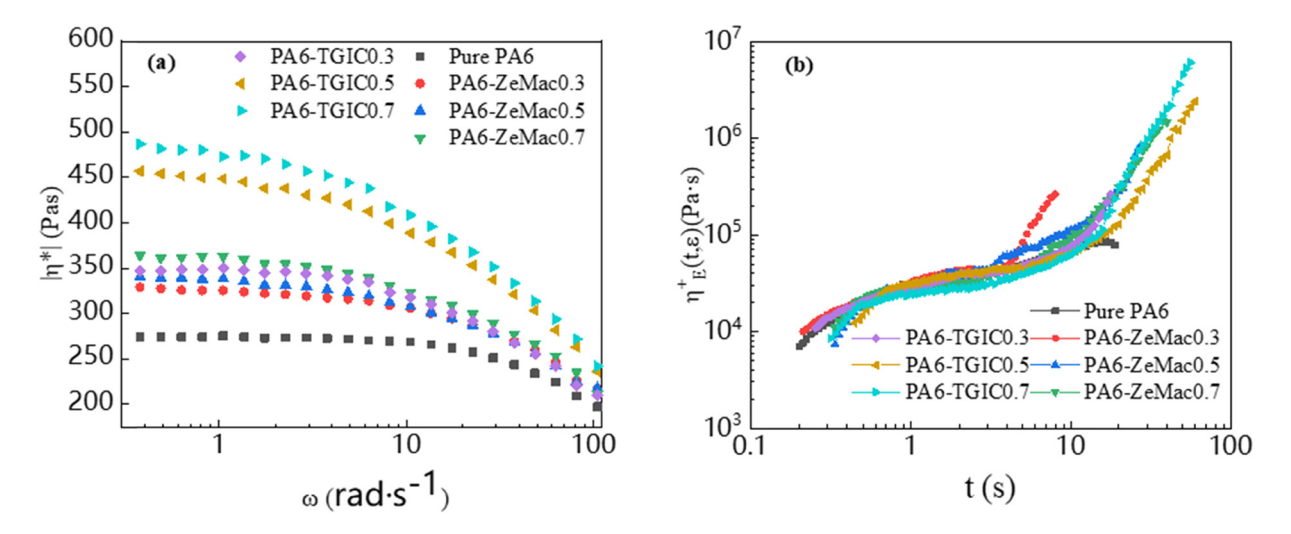


Figure 3: (a) The storage modulus G', (b) the loss modulus G'', and (c) the loss tangent tan  $\delta$  of pure PA6 and modified PA6 samples.



**Figure 4:** (a) Complex viscosity  $|\eta^*|$  and (b) tensile viscosity curves  $\eta_F^+$  of pure PA6 and modified PA6 samples.

of molecular chain, making it difficult to slip, which improves the viscoelasticity more significantly.

Figure 4a shows the complex viscosity ( $|\eta^*|$ ) of pure PA6 and its modified samples. All PA6 samples have typical shear thinning behavior with increasing shear rate. In addition, the complex viscosity increases with the increase of modifier content. This is attributable to the grafting and long-chain branching structure, which greatly improve the molecular chain entanglement and limit the movement of PA6 molecular chain. The dynamic shear rheology reflects the structural changes of PA6 to a certain extent, but the uniaxial tensile test is more sensitive to the molecular chain structure of the polymer. Figure 4b shows the variation curve of tensile viscosity ( $\eta_E^+$ ) of pure PA6 and its modified samples with time at a strain rate of 0.05 s<sup>-1</sup>. Pure PA6 has no strain hardening behavior. However, the addition of two modifiers makes

PA6 to undergo strain-induced hardening and, especially, the strain hardening of PA6-TGIC is more significant. The origin of strain hardening is macromolecular chain orientation and tension. The long-chain branching structure will form more macromolecular chain entanglements, resulting in greater stress in the process of strain (31). Strain hardening in the foaming process is conducive to increasing the viscosity with the development of strain, maintaining the stable growth of cell, preventing gas escape, and reducing the fracture and deformation of cell.

# 3.3 Crystallization properties

Figure 5 shows the cooling crystallization curve and heating melting curve of PA6-modified materials with different ZeMac and TGIC contents. Table 4 is the

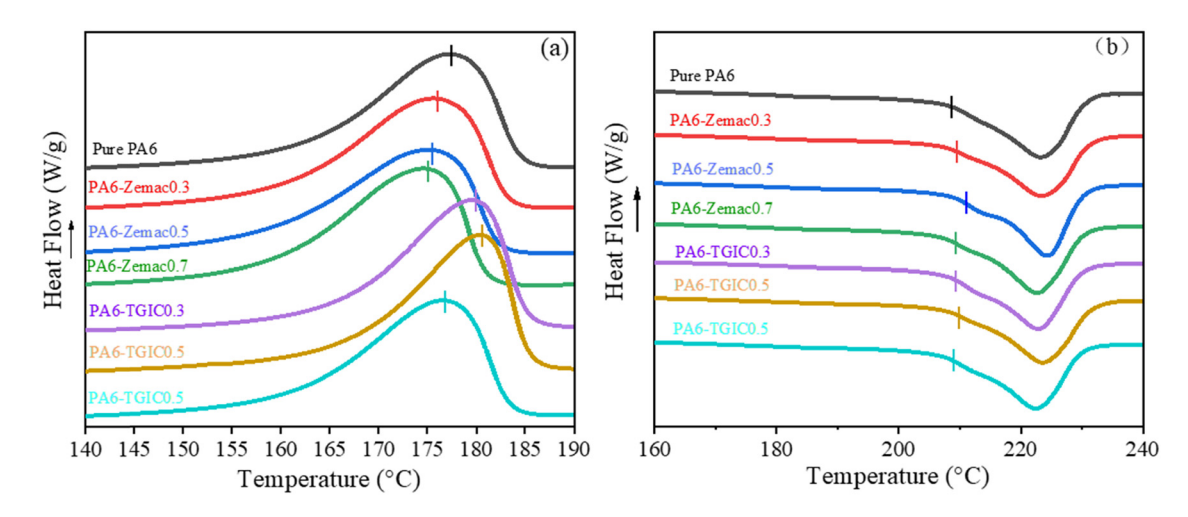


Figure 5: DSC graphs of pure PA6 and modified PA6 samples: (a) cooling crystallization curves and (b) heating melting curve.

Table 4: Crystallization and melting data of pure PA6 and modified PA6

Samples	Pure PA6	PA6-ZeMac0.3	PA6-ZeMac0.5	PA6-ZeMac0.7	PA6-TGIC0.3	PA6-TGIC0.5	PA6-TGIC0.7
T <sub>onset</sub> (°C)	184.5	183.3	182.2	181.9	185.2	186.4	183.4
$T_{\text{peak}}$ (°C)	177.2	175.8	175.3	174.5	179.5	180.4	176.6
T <sub>m</sub> (°C)	208.6	209.6	211.3	209.8	209.2	210.1	209.1
<i>X</i> <sub>c</sub> (%)	36.1	35.9	35.2	36.0	35.6	35.5	35.7

statistical data of Figure 5. It can be seen from the chart that the introduction of modifier ZeMac reduces the initial crystallization temperature  $T_{\rm onset}$  and crystallization peak temperature  $T_{\rm peak}$  of PA6. However, the introduction of modifier TGIC increases the  $T_{\rm onset}$  and crystallization peak temperature  $T_{\rm peak}$  of PA6. Combined with the POM (Figure A1 in Appendix), the blue part in the figure is the crystal part. The introduction of ZeMac delayed the time of crystal emergence but has little effect on the number

and size of crystals, indicating that ZeMac only delayed the formation of crystals do not affect the growth of crystals. The introduction of TGIC not only shortens the grain appearance time but also increases the number of PA6 grains and reduces the grain size, indicating that the introduction of TGIC increases the nucleation site and plays a role in grain refinement. The final crystallinity of PA6-TGIC changes little under the dual influence. The crystallization rates of the three samples from small

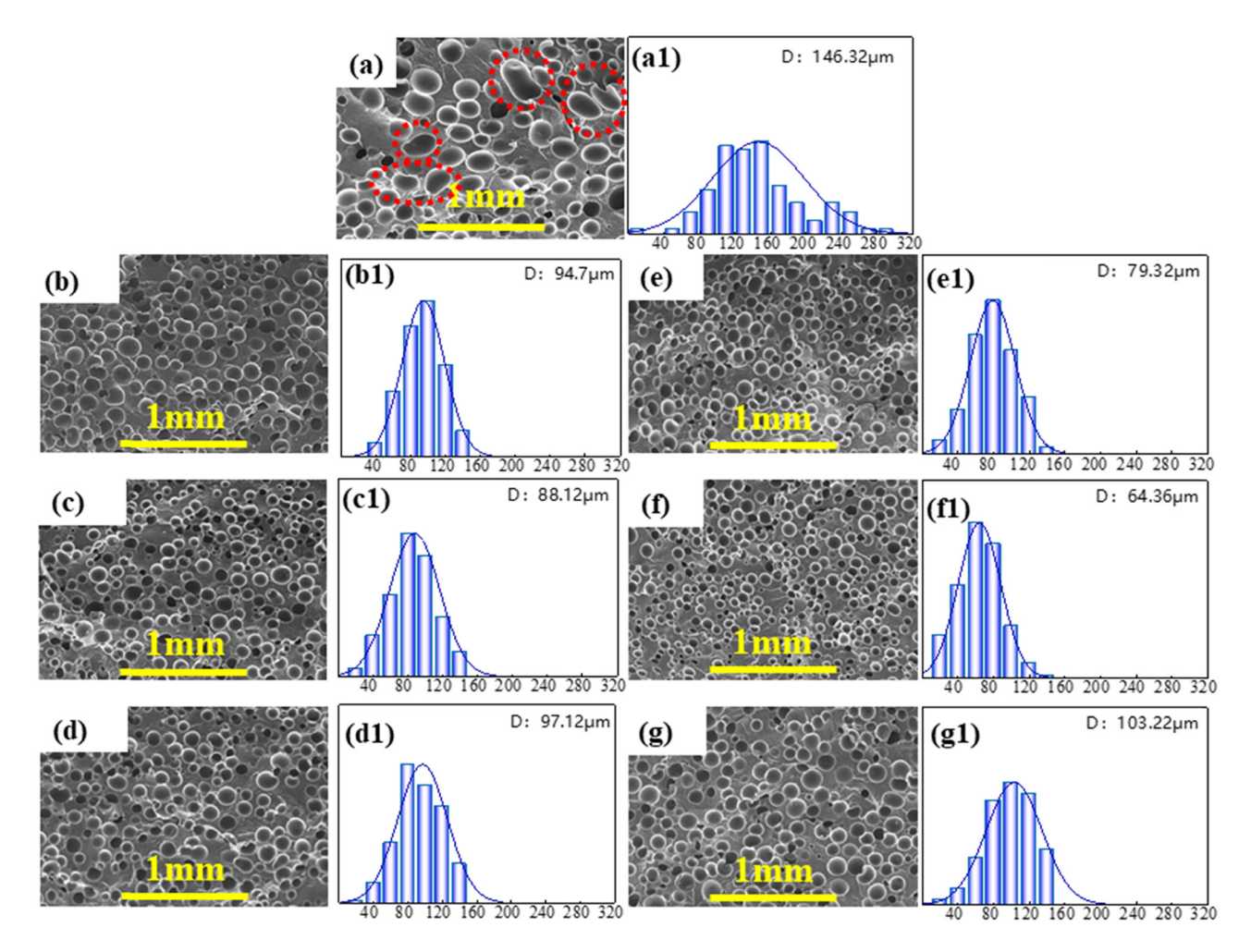


Figure 6: SEM images of microcellular foams and histogram of statistical distribution of microcell sizes in PA6 microcellular foams with different chain extender: pure PA6 (a,a1), PA6-ZeMac 0.3 (b,b1), PA6-ZeMac 0.5 (c,c1), PA6-ZeMac 0.7 (d,d1), PA6-TGIC 0.3 (e,e1), PA6-TGIC 0.5 (f,f1), PA6-TGIC 0.7 (g,g1).

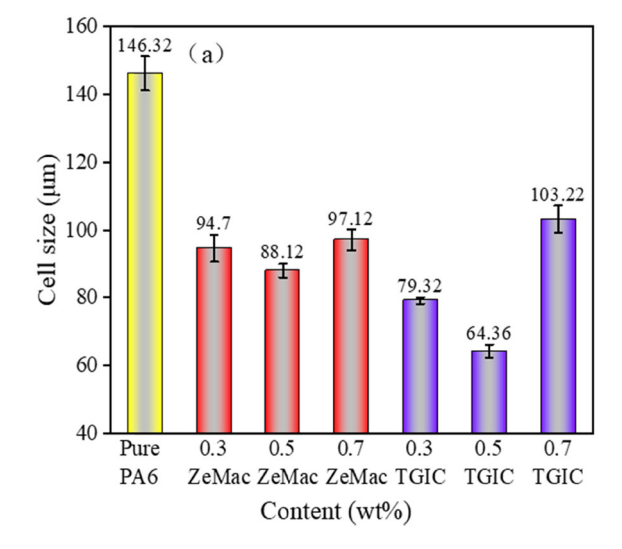
to large are respectively PA6-ZeMac 0.5, pure PA6, and PA6-TGIC 0.5 under conditions of isothermal crystallization. The difference of crystallization rates is caused by two different modification methods. For ZeMac as modifier, the crystallization rate is the slowest, which can be attributed to steric hindrance effects. Although the graft point as the crystallization nucleation point can promote crystallization, the steric hindrance effect of ZeMac molecular chain is large to cause PA6 molecular chain is difficult to fold, requiring a greater degree of undercooling and a longer time to complete crystallization.

For TGIC as modifier, it has little effect on the folding crystallization of PA6 molecular chain because of its low molecular weight and low steric hindrance effect (32–34). Therefore, the crystallization rate of PA6-TGIC is faster,  $T_{\rm onset}$  and  $T_{\rm peak}$  are increased.  $T_{\rm onset}$  and  $T_{\rm peak}$  begin to decrease when TGIC content is too high because the promotion of nucleation sites cannot compensate for the inhibition of reduced molecular chain activity. In addition, the melting temperature  $T_{\rm m}$  of the two modified materials increased because of the increased resistance of molecular chain movement in both modification methods according to Figure 5b.

# 3.4 Foaming performance

Figure 6 is the cell structure diagram after the introduction of two modifiers and the corresponding cell diameter distribution diagram. The cell size first decreases and then increases with the increase of the modifier content. The cell diameter distribution is in a normal distribution,

and with the introduction of the modifier, the cell size distribution becomes more uniform. Figure 7 is a graph of the average cell diameter and cell density of the two modifiers with different contents. The introduction of ZeMac reduced the average diameter of bubbles in pure PA6 from 146.32 to 88.12 µm, and the density of bubbles increased from  $1.69 \times 10^5$  to  $5.359 \times 10^5$  cells·cm<sup>-3</sup>. The introduction of TGIC reduced the average diameter of bubbles in pure PA6 from 146.32 to 64.36 µm, and the density of bubbles increased to 1.319  $\times$  10<sup>6</sup> cells·cm<sup>-3</sup>. When the modifier is not added, many cells of pure PA6 foamed material have been merging and deformed (inside the red dotted line in Figure 6a). The merging and deformation of pure PA6 cells disappeared after adding the modifier. According to the analysis of cell morphology (Figure A2), there are obvious cracks on the cell surface of pure PA6. The cell surfaces of PA6-ZeMac 0.5 and PA6-TGIC 0.5 are relatively complete, and the morphology is more regular than that of pure PA6. The above phenomena are mainly analyzed from the following two aspects. First, the melt viscoelasticity and melt strength of polyamide are improved by the two modification methods. The influence of the long-chain branching structure on the rheological behavior of materials is more significant than that of graft modification (Figures 4 and 5). More bubble nuclei can be expanded to form bubbles with the increase of viscoelasticity of melt and the deformation of bubbles is reduced. The increase of melt strength can reduce the excessive growth of bubbles and reduce the merging and rupture of bubbles (31). However, according to the classical nucleation theory, with the increase of melt viscosity, the resistance of cell nucleation increases, which will inhibit



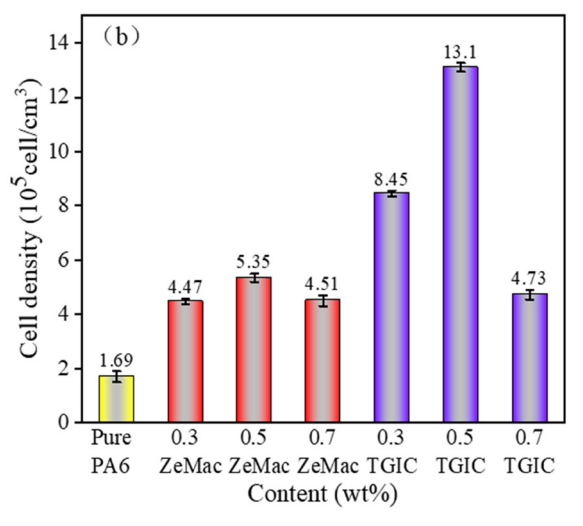


Figure 7: Average cell diameter (a) and cell density (b) of pure PA6 and modified PA6.

cell nucleation (35). Therefore, when the content of modifier is further increased, the cell density begins to decrease. Second, the branch point can be used as a crystal nucleation point to form a large number of crystal nuclei, which

increases the degree of molecular entanglement, inhibiting the mobility of molecules. Thus, the addition of modifiers plays a role in stabilizing cells and reduces cell rupture and deformation (36-38).

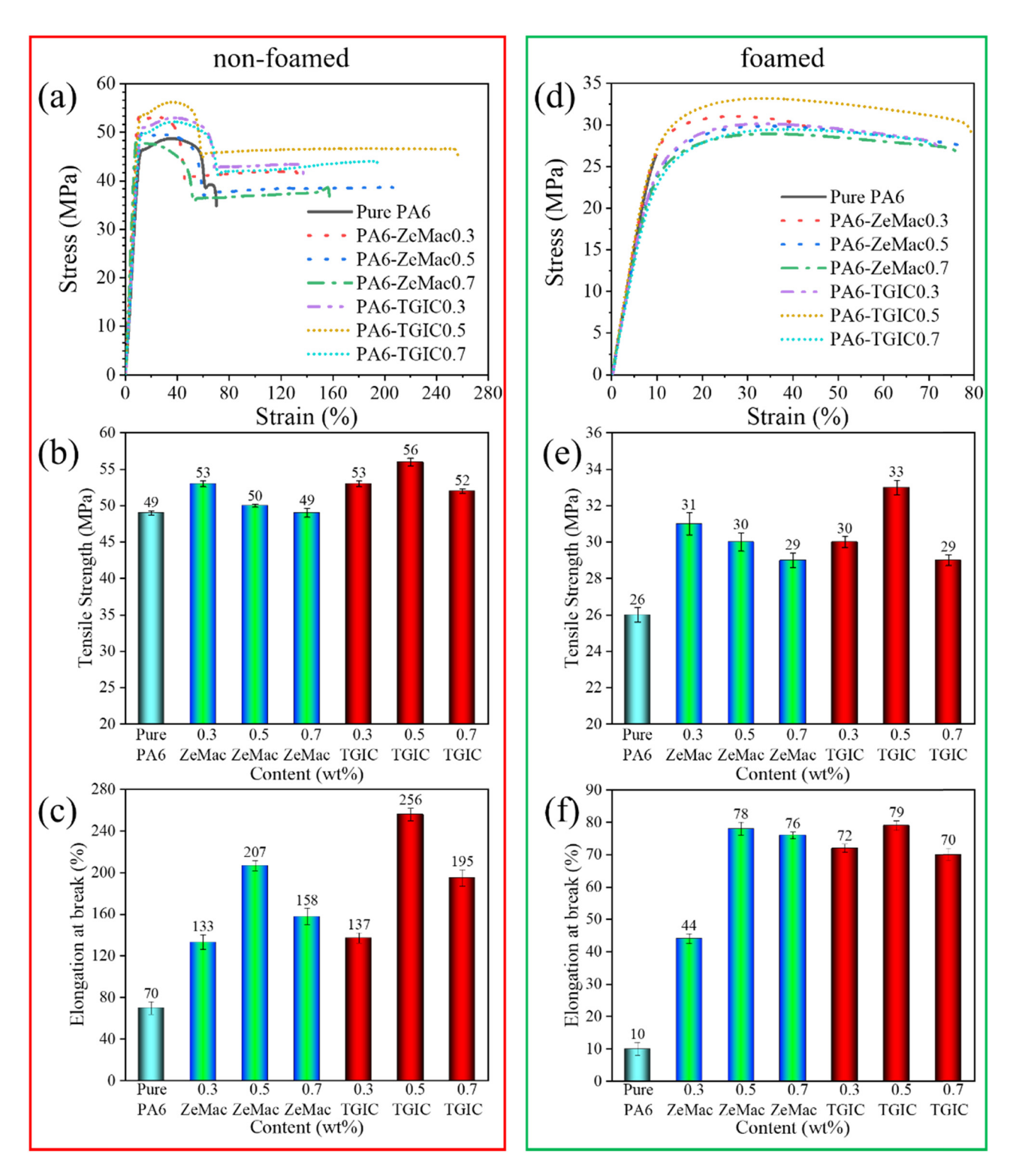


Figure 8: Tensile mechanical properties: (a and d) stress-strain curves, (b and e) tensile strength, and (c and f) elongation at break.

# 3.5 Mechanical properties

Figure 8 shows the change of the tensile properties of the nonfoamed sample and foamed sample of PA6 under two different modification methods. As shown in Figure 8, the tensile strength and elongation at break of the foamed sample are significantly reduced compared with nonfoamed sample due to the reduction of effective bearing area of foamed sample and defects caused by cell (19). With the addition of the modifier, the tensile strength and elongation at break of the nonfoamed and foamed PA6 samples are improved. In particular, the tensile properties of foamed samples have changed from brittle fracture without yield point to ductile fracture with yield point. The fracture tensile strain of PA6 modified by ZeMac increases from 10% to 78%, and the fracture tensile strain of PA6 modified by TGIC increases to 79%. Figure A3 shows the tensile cross-section of pure PA6, PA6-ZeMac 0.5, and PA6-TGIC 0.5 foam samples. The tensile fracture surface of pure PA6 foamed sample is smooth without obvious plastic deformation. Although there are some cracks on the cell surface, the overall cell morphology is relatively complete, indicating the brittle fracture behavior. The tensile fracture surface of PA6-ZeMac 0.5 and PA6-TGIC 0.5 foamed samples is rough, the cell has serious tensile deformation, and the resin has obvious tensile behavior in the tensile direction. This tensile can consume a lot of energy in the fracture process, indicating the ductile fracture behavior.

Figure 9 shows the impact strength changes of the nonfoamed sample and the foamed sample of PA6 under two different modification methods. The impact strength of the foamed sample is significantly reduced compared

with the nonfoamed sample due to the reduction of the effective bearing area of the foamed sample and the defects caused by the cell. With the addition of modifier, the impact strength of both nonfoamed and foamed samples of PA6 increased, and the impact strength of foamed samples increases further. Compared with nonfoamed samples, especially after long-chain branching modification, the impact strength of foamed samples increases from 4.1 to 7.8 kJ·m<sup>-2</sup>, an increase of 90.2%. This is because the foamed sample not only improves the toughness of the material itself, but also reduces the defects caused by large cell. Figure A4 shows the impact section of pure PA6, PA6-ZeMac 0.5, and PA6-TGIC 0.5 foam samples.

The reasons for the improvement of mechanical properties after modification are analyzed. First, grafting and long-chain branching structures increase the molecular weight and entanglement between molecular chains of PA6, which makes it difficult for the material to slip and disentangle between molecular chains in the process of tensile or impact, consumes more energy, and then increases the toughness of the material itself. LCB structures have better mechanical properties because they form more molecular chain entanglements than grafted structures. However, when the molecular chain is entangled too much, its mechanical properties will decline. This is attributable to the molecular chain has no time to move when the material is stretched or impacted due to the increase of the steric resistance of the molecular chain (27,39). Second, the finer and more uniform cell structure reduces the defects caused by the cell and brings higher strength to the material (40,41). In addition, the mechanical properties are highly related to density besides the cell structure.

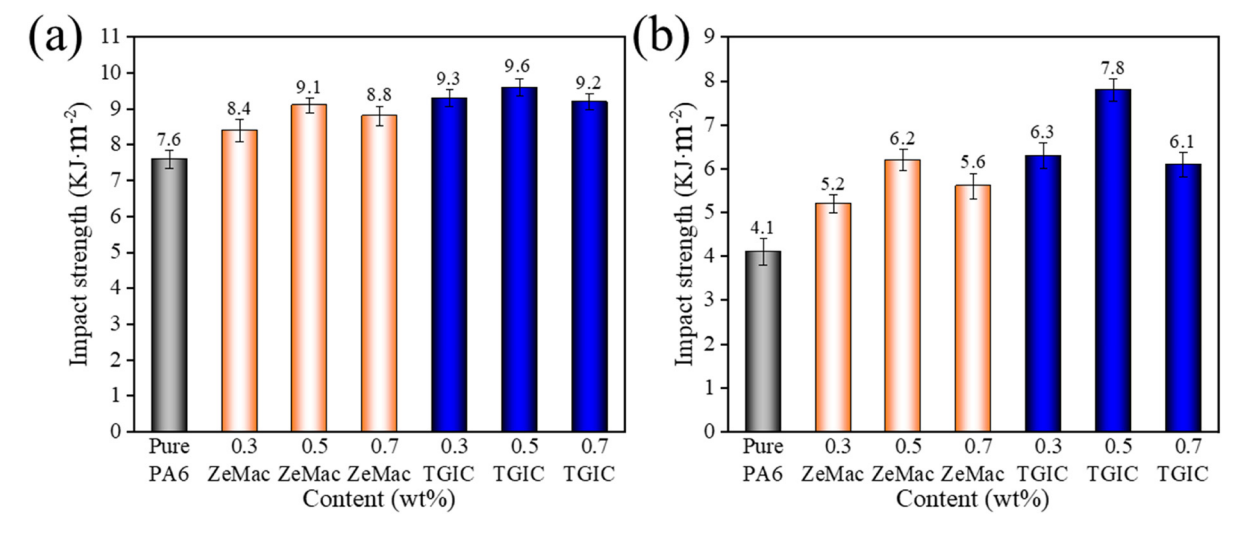


Figure 9: Impact strength of pure PA6 and modified PA6 foamed samples: (a) non-foamed and (b) foamed.

Figure A5 shows the density of nonfoamed samples and foamed samples. The density difference is small due to the same core-back distance. Therefore, the effect of density on the mechanical properties of materials can be ignored.

# 4 Conclusion

In this work, PA6 was modified with ZeMac and TGIC as modifiers to prepare a grafting structure and a longchain branching structure respectively. Subsequently, the effects of the two modification methods on the rheological behavior, crystallization properties, foaming performance, and mechanical properties of PA6 were discussed. The results showed that the effect of the long-chain branching structure on rheological behavior was more significant than that of the grafting structure. For the crystalline properties, grafting structure inhibited the formation of crystals and had little effect on the final size of crystals. Long-chain branching structure promoted the formation of crystals and reduced the final size of crystals. For foaming performance, compared with grafting modification, long-chain branching modification has finer and more uniform cell morphology. For mechanical properties, the foamed samples modified by long-chain branching have higher tensile and impact properties than those modified by grafting.

Acknowledgements: The authors would like to acknowledge the financial support of the National Natural Science Foundation of China (No. 51863003, No. 52063008), the Research Institute Service Enterprise Action Plan Project of Guizhou Province (No. [2018]4010), the Hundred Talents Project of Guizhou Province, Grant Number (No. [2016]5673), Key Projects of Guizhou Provincial Fund (No. ZK [2021]050, No. [2019]1176), and the Science and Technology Program of Guiyang City, Guizhou Province (No. [2019]14).

Funding information: National Natural Science Foundation of China (No. 51863003, No. 52063008), the Research Institute Service Enterprise Action Plan Project of Guizhou Province (No. [2018]4010), the Hundred Talents Project of Guizhou Province, Grant Number (No. [2016]5673), Key Projects of Guizhou Provincial Fund (No. ZK [2021]050, No. [2019]1176), and the Science and Technology Program of Guiyang City, Guizhou Province (No. [2019]14).

Author contributions: Lushuai Cao: writing - original draft, writing - review and editing, formal analysis; Li He: writing - original draft, formal analysis, project administration; Tuanhui Jiang: conceptualization; Bujin Liu: supervision; Ming Li: data curation; Di Zhang: data curation; Wei Gong: writing – original draft.

**Conflict of interest:** The authors state no conflict of interest.

**Data availability statement:** The datasets generated during and analyzed during the current study are available from the corresponding author on reasonable request.

# References

- Wang G, Zhao G, Zhang L, Mu Y, Park CB. Lightweight and tough (1) nanocellular PP/PTFE nanocomposite foams with defect-free surfaces obtained using in situ nanofibrillation and nanocellular injection molding. Chem Eng J. 2018;350:1-11.
- Qian M, Xu X, Qin Z, Yan S. Silicon carbide whiskers enhance mechanical and anti-wear properties of PA6 towards potential applications in aerospace and automobile fields. Compos B Eng. 2019;175:107096.
- (3) Mao H, He B, Guo W, Hua L, Yang Q. Effects of nano-CaCO3 content on the crystallization, mechanical properties, and cell structure of PP nanocomposites in microcellular injection molding. Polymers. 2018;10:1160.
- Mahmud MB, Anstey A, Shaayegan V, Lee PC, Park CB. Enhancing the mechanical performance of PA6 based composites by altering their crystallization and rheological behavior via in-situ generated PPS nanofibrils. Compos B Eng. 2020;195:108067.
- Li M, Qiu J, Xing H, Fan D, Wang S, Li S, et al. In-situ cooling of adsorbed water to control cellular structure of polypropylene composite foam during CO<sub>2</sub> batch foaming process. Polymers. 2018;155:116-28.
- Wang L, Wan D, Qiu J, Tang T. Effects of long chain branches on the crystallization and foaming behaviors of polypropylene-gpoly(ethylene-co-1-butene) graft copolymers with welldefined molecular structures. Polymer. 2012;53:4737-57.
- (7) Yao S, Guo T, Liu T, Xi Z, Xu Z, Zhao L. Good extrusion foaming performance of long-chain branched PET induced by its enhanced crystallization property. J Appl Polym Sci. 2020;137(41):0021-8995.
- Jiang TH, Zhang H, Zeng XB, Zhang C, Gong W, He L. The effect of injection process for microcellular foaming on the cell morphology and surface quality of polyamide 6. Mater Res Express. 2021;8(4):045311.
- (9) Xu MJ, Liu HC, Ma K, Li B, Zhang ZY. New strategy towards flame retardancy through design, synthesis, characterization, and fire performance of a chain extender in polyamide 6 composites. Polym Eng Sci. 2019;59(s2):E206-15.
- (10) Wu G, Xu Y, Chen J, Dang K, Yang W, Xie P. In situ fibrillationreinforced polypropylene-based multi-component foams. Polym Adv Technol. 2021;32:4052-60.
- (11) Deng R, Zhang C, Liu BJ, Jiang TH. Effect of elastomer on foaming behavior of micro foamed polypropylene composites. Polym Mater Sci Eng. 2021;37(2):80-8.
- (12) He Y, Yang HM, Zhang C, Jiang TH, He L, Gong W. Foaming behavior of polypropylene/inorganic nano-particle composites. Polym Bullet. 2016;4:80-7.

- (13) Ren X, Tu Z, Wang J, Jiang T, Yang Y, Hu GH. Critical rubber layer thickness of core-shell particles with a rigid core and a soft shell for toughening of epoxy resins without loss of elastic modulus and strength. Compos Sci Technol. 2017;153:253-60.
- (14) Liu Y, Wang Y, Zhang C, Liu T. 2D nanosheet-constructed hybrid nanofillers for polymer nanocomposites with synergistic dispersion and function. APL Mater. 2019;7(8):080904.
- (15) Xu Z, Lin X, Luo C, Xiao W. The application of a tri-functional epoxy resin as a crosslinking agent in extruded polyamide-6 foam. Polym Sci Ser B+. 2019;61(5):574-81.
- (16) Li Y, Pan C, Xin Z, Zhou S, Meng X, Zhao S. Rheological, crystallization and foaming behaviors of high melt strength polypropylene in the presence of polyvinyl acetate. J Polym Res. 2018;25(2):46.
- (17) Xu M, Lu J, Zhao J, Wei L, Liu T, Park CB. Rheological and foaming behaviors of long-chain branched polyamide 6 with controlled branch length. Polymer. 2021;224:123730.
- (18) Leng X, Wei Z, Bian Y, Wang Y, Wang Q, Li Y. Rheological properties and crystallization behavior of comb-like graft poly (L-lactide): influences of graft length and graft density. RSC Adv. 2016;6:30320-29.
- (19) Zong Q, Xu A, Chai K, Zhang Y, Song Y. Increased expansion ratio, cell density, and compression strength of microcellular poly (lactic acid) foams via lignin graft poly (lactic acid) as a biobased nucleating agent. Polym Adv Technol. 2020;31(10):2239-49.
- (20) Zhao J, Wang Z, Wang H, Zhou G, Nie H. High-expanded foams based on novel long-chain branched poly (aryl ether ketone) via ScCO2 foaming method. Polymer. 2019;165:124-32.
- (21) Jiang R, Chen Y, Yao S, Xu Z, Park CB, Zhao L. Preparation and characterization of high melt strength thermoplastic polyester elastomer with different topological structure using a two-step functional group reaction. Polymer. 2019;179:121628.
- (22) Li Y, Yao Z, Qiu S, Zeng C, Cao K. Influence of molecular structure on the rheological properties and foamability of long chain branched polypropylene by "one-pot" reactive extrusion. J Cell Plast. 2020;57(4):433-49. doi: 0021955X2094310.
- (23) Lai D, Li Y, Wang C, Liu Y, Li D, Yang J. Inhibition effect of aminated montmorillonite on crystallization of dendritic polyamide 6. Mater Today Commun. 2020;25:101578.
- (24) Xu M, Chen Y, Liu T, Zhao L, Park CB. Determination of modified polyamide 6's foaming windows by bubble growth simulations based on rheological measurements. J Appl Polym Sci. 2019;136(42):4838.
- (25) Wang G, Zhao J, Yu K, Mark LH, Wang G, Gong P, et al. Role of elastic strain energy in cell nucleation of polymer foaming and its application for fabricating sub-microcellular TPU microfilms. Polymer. 2017;119:28-39.
- (26) Forest C, Chaumont P, Cassagnau P, Swoboda B, Sonntag P. Nanofoaming of PMMA using a batch CO<sub>2</sub> process: influence of the PMMA viscoelastic behaviour. Polymer. 2015;77:1-9.
- Wang G, Zhao G, Wang S, Zhang L, Park CB. Injection-molded microcellular PLA/graphite nanocomposites with dramatically enhanced mechanical and electrical properties for ultra-

- efficient EMI shielding applications. J Mater Chem C. 2018;6:6847-59.
- (28) Zhao J, Wang G, Zhang L, Li B, Wang C, Zhao G, et al. Lightweight and strong fibrillary PTFE reinforced polypropylene composite foams fabricated by foam injection molding. Eur Polym J. 2019;119:22-31.
- (29) Liu J, Lou L, Yu W, Liao R, Li R, Zhou C. Long chain branching polylactide: structures and properties. Polymer. 2010;51(22):5186-97.
- (30) Liu W, Wu X, Ou Y, Liu H, Zhang C. Electrically conductive and light-weight branched polylactic acid-based carbon nanotube foams. e-Polymers. 2021;21(1):96-107.
- (31) Liu B, Jiang T, Zeng X, Deng R, Gu J, Gong W, et al. Polypropylene/thermoplastic polyester elastomer blend: crystallization properties, rheological behavior, and foaming performance. Polym Adv Technol. 2021;32(5):2102-17.
- (32) Li Y, Mi J, Fu H, Zhou H, Wang X. Nanocellular foaming behaviors of chain-extended poly (lactic acid) induced by isothermal crystallization. ACS omega. 2019;4(7):12512-23.
- (33) Buccella M, Dorigato A, Pasqualini E, Caldara M, Fambri L. Chain extension behavior and thermo-mechanical properties of polyamide 6 chemically modified with 1,1'-carbonyl-biscaprolactam. Polym Eng Sci. 2014;54(1):158-65.
- (34)Liu H, Zhang B, Zhou L, Li J, Zhang J, Chen X, et al. Synergistic effects of cellulose nanocrystals-organic montmorillonite as hybrid nanofillers for enhancing mechanical, crystallization, and heat-resistant properties of three-dimensional printed poly(lactic acid) nanocomposites. Polym Eng Sci. 2021;61:122-32.
- (35) Yang J, Jiang T, Liu B, Zhang C, Zeng X, He L, et al. Experimental and numerical analysis of bubble nucleation in foaming polymer. Mater Des. 2021;2:109577.
- (36) Yang Y, Li X, Zhang Q, Xia C, Chen C, Chen X, et al. Foaming of poly (lactic acid) with supercritical CO2: The combined effect of crystallinity and crystalline morphology on cellular structure. J Supercrit Fluids. 2019;145:122-32.
- (37) Wang J, Zhu W, Zhang H, Park CB. Continuous processing of low-density, microcellular poly(lactic acid) foams with controlled cell morphology and crystallinity. Chem Eng Sci. 2012;75(none):390-9.
- (38) Zhou Y, He L, Gong W. Effects of zinc acetate and cucurbit[6] uril on PP composites: crystallization behavior, foaming performance and mechanical properties. e-Polymers. 2018;18(6):491-9.
- (39) Xu M, Lu J, Qiao Y, Wei L, Liu T, Lee PC, et al. Toughening mechanism of long chain branched polyamide 6. Mater Des. 2020;196:109173.
- (40) Gong W, Jiang TH, Zeng XB, He L, Zhang C. Experimentalnumerical studies of the effect of cell structure on the mechanical properties of polypropylene foams. e-Polymers. 2020;20(1):713-23.
- (41) Zou L, Li H, Wang D, Ma L, Zhang ZX. Micro/nanocellular polyprolene/trans-1,4-polyisomprene (PP/TPI) blend foams by using supercritical nitrogen as blowing agent. Polym Eng Sci. 2019;60(3):1-7.

# **Appendix**

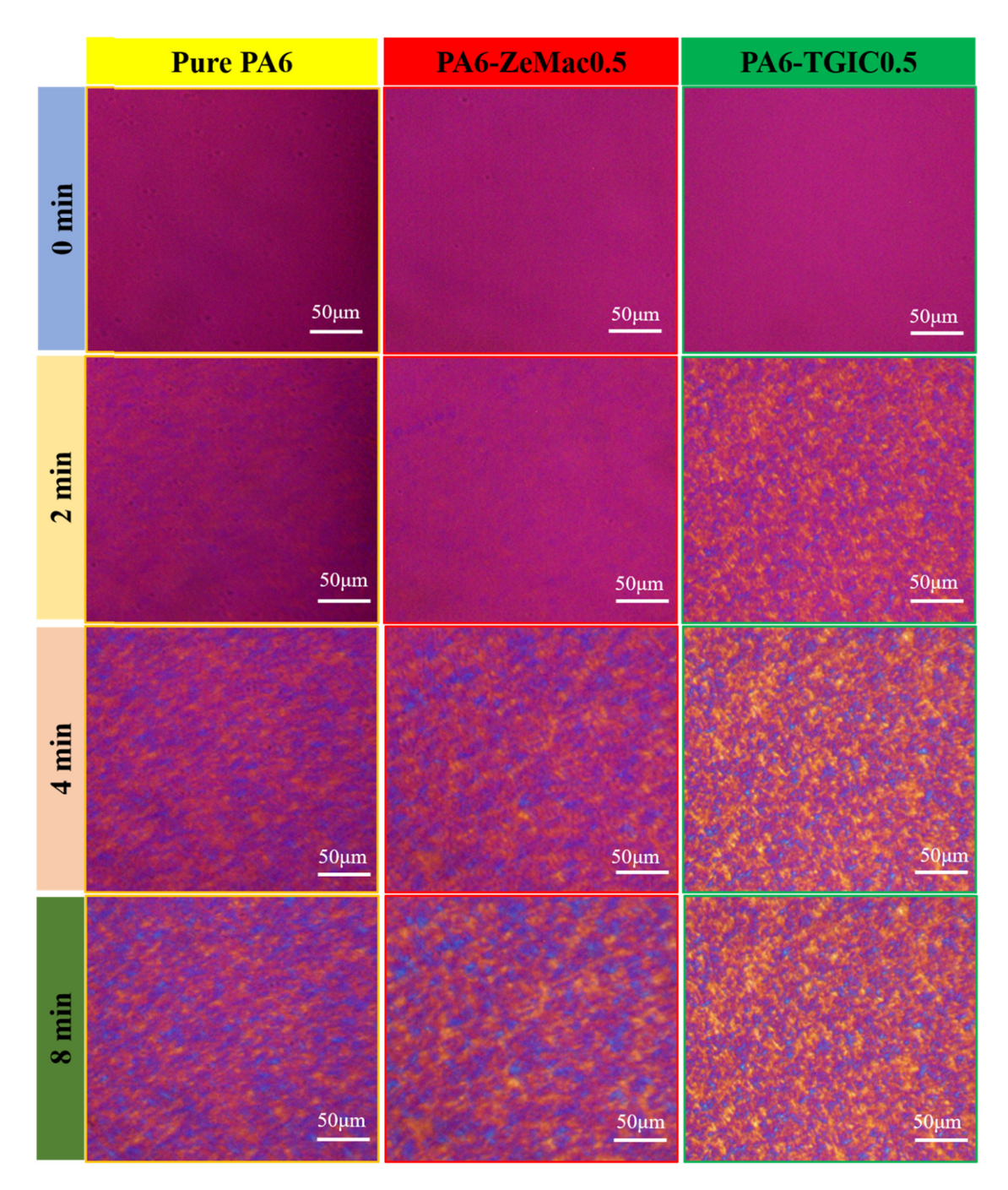


Figure A1: POM images of pure PA6, PA6-ZeMac 0.5, and PA6-TGIC 0.5 isothermally crystallized at 195°C.

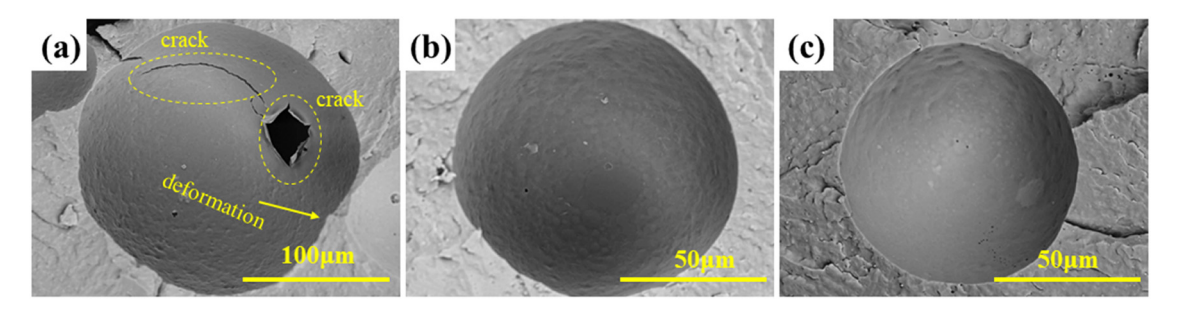


Figure A2: Cell microscopic morphology of (a) pure PA6, (b) PA6-ZeMac 0.5, and (c) PA6-TGIC 0.5.

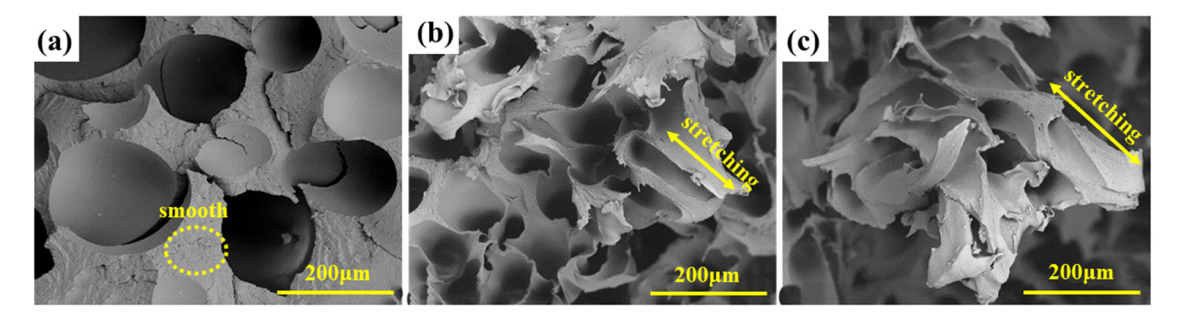


Figure A3: Tensile fracture surfaces of (a) pure PA6, (b) PA6-ZeMac 0.5, and (c) PA6-TGIC 0.5.

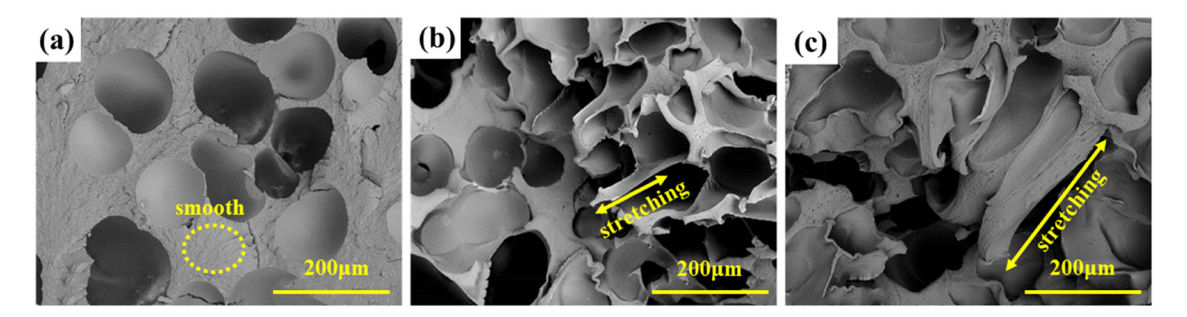


Figure A4: Impact fracture surfaces of (a) pure PA6, (b) PA6-ZeMac 0.5, and (c) PA6-TGIC 0.5.

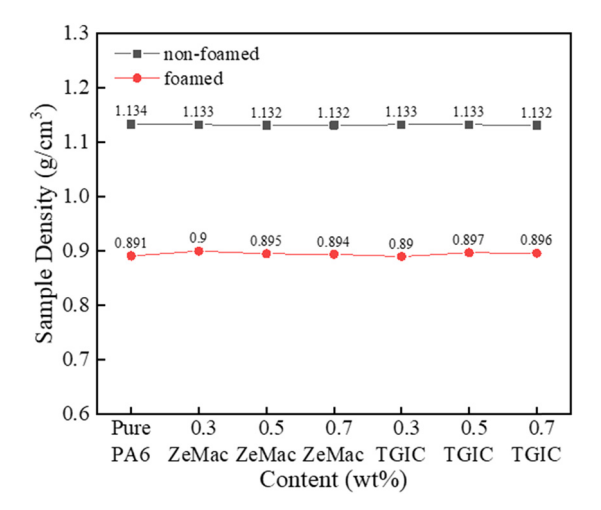


Figure A5: Density of nonfoamed samples and foamed samples.